Improving Time-Domain Measurements with a Network Analyzer Using a Robust Rational Interpolation Technique

Wendemagegnehu T. Beyene, *Member, IEEE*

***Abstract*—A method to efficiently and accurately compute a time-domain waveform from a network-analyzer frequency-domain measurement is presented in this paper. The method is based on a robust interpolation technique to construct a pole-residue representation of the response of the device-under-test. First, the rational function is expressed in terms of Chebyshev polynomials, instead of the usual power series, to accurately determine the poles of the network over a wide frequency range. The properties of a passive system are then utilized to efficiently calculate the residues. The resulting pole-residue model is analytically transformed to obtain the time-domain response in any time window, beyond the limitations of the discrete Fourier transform (DFT) technique. Unlike the DFT technique, the method does not require a large number of equally spaced harmonically related frequency points. The parametric model can also be used to economically store large measurement data. The proposed procedure is computationally inexpensive and less sensitive to numerical instability. To illustrate the validity of the method, examples of frequency- and time-domain measurements of a Beatty structure and simulation data of a low-pass Butterworth filter are given.**

***Index Terms*—Chebyshev polynomial, Fourier transform, Laplace transform, network analyzer, pole-residue model, rational interpolation, scattering parameter.**

I. Introduction

SCATTERING parameters of complex structures and devices can be measured with high accuracy using one of the commercially available network analyzers. These measured frequency-domain data can then be transformed to the time domain using the inverse discrete Fourier transform (IDFT). The resulting waveforms can then be used to characterize a network in the time domain. Therefore, the time-domain waveform can benefit from the wide dynamic range, error correction techniques of the frequency-domain data, better signal-to-noise ratio, and freedom form time jitter and zero-level drift [1].

For example, the Agilent 8510B network analyzer, with the built-in time-domain option, translates wide-band frequency-domain measurement data into a time-domain response through the use of a chirp-z transform [2]. Thus, such network analyzers can perform traditional time-domain reflectrometry (TDR) and time-domain transmission (TDT) measurements. These TDR and TDT measurements provide the time-domain behaviors of the device-under-test (DUT) in terms of step and impulse responses, respectively, that are often useful for such applications as signal integrity analysis.

Traditionally, the fast Fourier transform (FFT) is used to transform measurement data between frequency and time domains. Although the FFT offers faster computational speed, it limits the resolution of the time-domain response. The time-domain increment limitation of the FFT can be removed by using more expensive Fourier transform techniques. For example, although the chirp-z transform takes about four times longer than the FFT, it provides a compromise between the FFT and the direct use of the Fourier transform in terms of efficiency and flexibility [3]. In addition, the transform of data between the domains require the application of an artificial band limiting filter in order to avoid ringing, overshoot (Gibbs' phenomenon), and aliasing in the time domain.

Recently, several new methods have been proposed to improve the resolution and accuracy of the time-domain response obtained from frequency-domain measurements [4]–[7]. In [4], a generalized pencil of function technique is introduced to locate the impulses representing reflections due to discontinuities that would not have been resolved using the discrete Fourier transform (DFT). The method is able to extract an impulse response of a system out of a limited frequency bandwidth data. This parametric technique uses singular value decomposition to determine the dominant poles of the network. In [5], a parametric model is constructed from the frequency-domain data to improve the time-domain resolution of a vector-network analyzer. The data is modeled as a superposition of modulated complex sinusoids through optimization of a sequence of cost functions. In [6], a parametric time-domain technique is used to model the behavior of a microwave network from a set of frequency samples. The method is based on modeling the frequency-domain data as a rational function in the z-domain. In [7], model-based spectral analysis is also used to improve the resolution of the frequency-domain data beyond the limitations of the DFT. This technique is used to obtain high-resolution spectral details from fewer samples. The values of the coefficients are determined using covariance and principal component autoregressive methods. The methods in [4]–[7], however, are computationally very expensive and the models lack accuracy to fully represent the time-domain behaviors of the DUT.

In this paper, an efficient and accurate method to compute the time-domain response from frequency-domain data is presented. A robust rational interpolation technique is used to generate a pole-residue representation that can be transformed analytically to the time domain without any distortion. The com-

Manuscript received November 8, 1999.

The author was with Agilent Technologies, Westlake Village, CA 91362 USA. He is now with Rambus Inc., Los Altos, CA 94022 USA (e-mail: wbeyene@rambus.com).

Publisher Item Identifier S 0018-9480(01)01685-4.

plexity of the method involves solutions of two linear systems of equations and one factorization of a real polynomial. The method does not involve any derivatives of the response. Unlike previously proposed methods [4]–[7], it neither requires optimization, nor the solutions of eigenvalue problems, nor the singular value decomposition of the data matrix.

In Section II, scattering parameter formulation of linear networks are reviewed. In Section III, the robust rational interpolation technique is discussed, and the procedure for the time-domain measurement is presented in Section IV. Experimental results and conclusion are given in Sections V and VI, respectively.

II. Scattering-Parameter Formulation

Although impedance, admittance, and hybrid parameters are commonly used to characterize networks, they are difficult to measure accurately at high frequencies. They can take extreme values—tend to minus or plus infinity—or even not exit, i.e., they can be singular, at resonance frequencies of the DUT. However, scattering parameters, in addition to their unique physical meaning, remain bounded and stable. They are suitable at high frequencies where traveling-wave concepts predominate over lumped-element techniques. In addition, a scattering matrix exists for every linear, passive, and time-invariant network and are readily available from high-frequency measurements. The frequency-domain scattering matrix relates incident to the reflected waves as

$$B(s) = S(s)A(s) \tag{1}$$

where $S(s)$ is the scattering matrix describing the system and $A(s)$'s and $B(s)$'s are the forward and backward traveling-wave vectors, respectively, in the Laplace domain. The main diagonal entries of $S(s)$ are reflection coefficients and those along the off-diagonal are transmission coefficients. The time-domain formulation is given as

$$b(t) = s(t) * a(t) \tag{2}$$

where $s(t)$ is a time-domain scattering matrix describing the system, $a(t)$'s and $b(t)$'s are the forward and backward time-domain traveling wave vectors, respectively, and $*$ is used to denote convolution.

A scattering parameter of a passive system can be approximated by a least minimum error using a rational function because it captures the behavior of networks around its poles. Its partial fraction expansions can also readily be used to obtain the time-domain responses as sums of trigonometric and/or exponential functions. The characteristic function of an arbitrary passive network can have an infinite number of poles; however, it can be approximated by a finite-order rational function of degree (ε/ϑ). By choosing an appropriate reference system, the accuracy of the approximation can even be improved. The rational function matrix that interpolates the n-port scattering matrix at given points can be written as

$$H(s) = \frac{Q_\varepsilon(s)}{P_\vartheta(s)} = \frac{A_0 + A_1 s + A_2 s^2 + \cdots + A_\varepsilon s^\varepsilon}{1 + b_1 s + b_2 s^2 + \cdots + b_\vartheta s^\vartheta} \tag{3}$$

where b_0 is normalized to unity. The A_i's are the $n \times n$ coefficient matrices of the numerator polynomials of the scattering parameters and b_i's are the coefficients of the denominator polynomial common to the scattering parameters. For each transfer parameter $H_{ij}(s)$, (3) contains $r = \varepsilon + \vartheta + 1$ free coefficients, hence, at most, r independent parameters.

This rational function can be expressed in partial fraction expansion of the form

$$H(s) = K_0 + \sum_{i=1}^{\vartheta} \frac{K_i}{s - p_i} \tag{4}$$

where the p_i's are the common poles and K_i's are residues of the scattering matrix.[1] The inverse Laplace transform of (4) yields the time-domain impulse response $h(t)$ written as

$$h(t) = K_0 \delta(t) + \sum_{i=1}^{\vartheta} K_i e^{p_i t}. \tag{5}$$

The step response of the system $g(t)$ is also given as

$$g(t) = K_0 u(t) + \sum_{i=1}^{\vartheta} \left(\frac{K_i}{p_i} e^{p_i t} - \frac{K_i}{p_i} u(t) \right) \tag{6}$$

where $u(t)$ is a unit step function. Similar expressions are also available for high-order stimuli. Now that the system response is expressed as a sum of exponential terms, the response to arbitrary stimulus can be efficiently obtained from (5) or (6) by taking advantage of recursive convolution [8], [9].

III. Robust Rational Interpolation

The coefficients of the rational function in (3) are determined so that the approximating function evaluated at the same frequency points give close approximation to the function $H(s)$. By canceling the denominator in (3) and evaluating the equation at the samples of the scattering parameters $S[i] = H(s_i)$ and k specified distinct points s_i, $i = 0, \ldots, k-1$, the resulting equations give a linear homogenous system of k equations in r unknowns

$$Q_\varepsilon(s_i) - P_\vartheta(s_i) S_i = 0. \tag{7}$$

This equation can be written in a matrix form as (8), shown at the bottom of the following page.

The approximation problem can be solved more efficiently and accurately by utilizing the special properties of passive systems. For instance, constraints necessary to insure a physically realizable passive network require that the transfer function be a rational fraction of polynomials in s. The coefficients of these polynomials must be real, and all roots of the denominator polynomial must have negative or zero real parts. Thus, the response of a passive network can only decay in time from any transient initial state. In addition, network functions are analytic functions of a complex variable; hence, their real and imaginary parts are related by Cauchy–Riemann equations and are Hilbert transform of each other [10]. For example, the frequency variations

[1]The multiplicity of the approximate poles $|p_i - p_j| > \epsilon$ can be assumed to be single without any loss of generality.

of resistance and reactance or conductance and sucepectance of an electrical network are not arbitrary. They are related through Hilbert transform, just as in the Kramers–Kröning relations between real and imaginary parts of permittivity and permeability [11]. This is because the poles of passive network functions are constrained to the left half-s-plane, the zeros of impedance and admittance functions are too located in this half-plane, and that this functions are analytic in the left half-plane. This relation assures the causality of the time-domain response [12]. The consequence of this property is that only the real part or imaginary part of the network function has to be approximated and the network function itself can be found from the resulting approximation [13], [14].

The real part of the network function in (3) can be specified as the even part of $H(s)$ replacing $-s^2$ by ω^2. Consequently, the real part of the original function is fitted with the real rational polynomial function of the squared variable. Since the poles of the even function $H(s)$ are those of both $H(s)$ and $H(-s)$, the poles belonging to $H(s)$ lie in the left complex frequency half-plane. Thus, the denominator coefficients in (3) can be obtained from the even part of $H(s)$. By matching the real parts of the original function with (3) at the set of frequencies, system of equations results are shown in (9) at the bottom of this page.

Note that (9) can be solved for the corresponding numerator coefficient matrices and denominator coefficients A's and b's, respectively. For higher order approximations over a wider frequency range, the system in (9) is highly ill conditioned and nearly singular when the frequency range is wide or the order of the approximation is high. This is because the ordinary power series $\{\omega^0, \omega^1, \omega^2, \omega^3, \ldots\}$ have a very large dynamic range, and they become almost parallel at higher orders. As shown in Fig. 1, for higher orders, the shapes of the power series become very similar over most of the normalized frequency range [15]. In [14], several techniques have been suggested to improve the accuracy of the solution for this ill-conditioned system of equations.

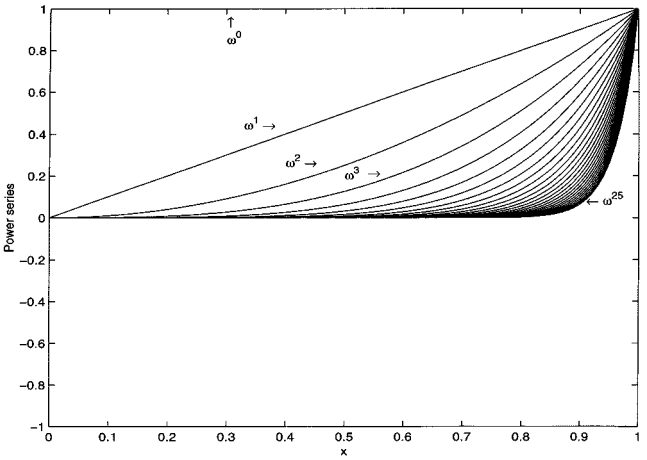

Fig. 1. Shapes of the power series ω^0 through ω^{25} become very similar for high orders over most of the normalized frequency range.

$$\begin{bmatrix} 1 & s_0 & s_0^2 & \cdots & s_0^{\varepsilon} & -s_0S_0 & -s_0^2S_0 & \cdots & -s_0^{\vartheta}S_0 \\ 1 & s_1 & s_1^2 & \cdots & s_1^{\varepsilon} & -s_1S_1 & -s_1^2S_1 & \cdots & -s_1^{\vartheta}S_1 \\ \vdots & \vdots & \vdots & \ddots & \vdots & \vdots & \vdots & \ddots & \vdots \\ 1 & s_{k-1} & s_{k-1}^2 & \cdots & s_{k-1}^{\varepsilon} & -s_{k-1}S_{k-1} & -s_{k-1}^2S_{k-1} & \cdots & -s_{k-1}^{\vartheta}S_{k-1} \end{bmatrix} \begin{bmatrix} A_0 \\ A_1 \\ A_2 \\ \vdots \\ A_{\varepsilon} \\ b_1 \\ b_2 \\ \vdots \\ b_{\vartheta} \end{bmatrix} = \begin{bmatrix} S_0 \\ S_1 \\ S_2 \\ \vdots \\ S_{k-1} \end{bmatrix} \tag{8}$$

$$\begin{bmatrix} 1 & \omega_0^2 & \cdots & \omega_0^{2\varepsilon} & -\omega_0^2\mathrm{Re}(S(\omega_0)) & \cdots & -\omega_0^{2\vartheta}\mathrm{Re}(S(\omega_0)) \\ 1 & \omega_1^2 & \cdots & \omega_1^{2\varepsilon} & -\omega_1^2\mathrm{Re}(S(\omega_1)) & \cdots & -\omega_1^{2\vartheta}\mathrm{Re}(S(\omega_1)) \\ \vdots & \vdots & \ddots & \vdots & \vdots & \ddots & \vdots \\ 1 & \omega_{k-1}^2 & \cdots & \omega_{k-1}^{2\varepsilon} & -\omega_{k-1}^2\mathrm{Re}(S(\omega_{k-1})) & \cdots & -\omega_{k-1}^{2\vartheta}\mathrm{Re}(S(\omega_{k-1})) \end{bmatrix} \begin{bmatrix} A_0 \\ A_1 \\ \vdots \\ A_{\varepsilon} \\ b_1 \\ \vdots \\ b_{\vartheta} \end{bmatrix} = \begin{bmatrix} \mathrm{Re}(S(\omega_2)) \\ \mathrm{Re}(S(\omega_2)) \\ \mathrm{Re}(S(\omega_2)) \\ \vdots \\ \mathrm{Re}(S(\omega_{k-1})) \end{bmatrix} \tag{9}$$

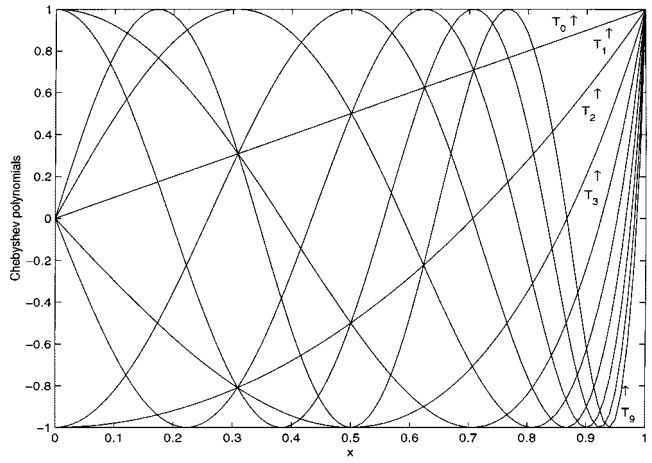

Fig. 2. Chebyshev polynomials $T_0(\omega)$ through $T_9(\omega)$ have different shapes over most of the normalized frequency range.

Another approach to circumvent the ill-conditioned matrix in (9) is to use orthogonal polynomials instead of ordinary power series. The Chebyshev polynomial of degree k is denoted $T_k(x)$ and is given by the explicit formula

$$T_k(x) = \cos(n \arccos x). \tag{10}$$

For a Chebyshev polynomial of degree k, there is an equivalent kth-order power series

$$\begin{aligned} T_0(x) &= 1 \\ T_1(x) &= x \\ T_2(x) &= 2x^2 - 1 \\ T_3(x) &= 4x^3 - 3x \\ &\vdots \\ T_{k+1}(x) &= 2xT_k(x) - T_{k-1}(x), \qquad n \geq 1. \end{aligned} \tag{11}$$

As shown in Fig. 2, the Chebyshev polynomials have quite different shapes over most of the normalized frequencies where they will be used [15]. They are orthogonal in the interval $[-1, 1]$ over a weight $(1 - x^2)^{-1/2}$. In addition, Chebyshev polynomials have a small dynamic range that is bounded between -1 and 1 in the interval $[-1, 1]$. This makes the Chebyshev polynomials particularly well suited for very high-order interpolation problems. Therefore, Chebyshev polynomials give better accuracy.

Equation (9) can be rewritten using the Chebyshev polynomials of (12), shown at the bottom of this page. Thus, after solving for the coefficients $\tilde{A}$'s and $\tilde{b}$'s of the Chebyshev polynomials, the equivalent coefficients of the same order power series can be found. Clenshaw's recurrence formula can be used to efficiently calculate the coefficients [16].

After the coefficients are converted to coefficients of the ordinary power series, the zeros of the denominator polynomial are found using one of the polynomial root-finder techniques [16]. Factoring the denominator and taking only the left half-plane poles, the partial fraction is constructed. No unstable (positive) poles are obtained since the polynomial roots are determined in terms of the squared poles. These stable poles are used to calculate the residues by matching the real and imaginary parts of the partial fraction expression of the transfer faction in (4) to the original frequency-domain data at a set of points. Equation (4) can be rewritten into real and imaginary parts as follows:

$$S(\omega) = \left(K_0 - \sum_{i=1}^{\vartheta} \frac{K_i p_i}{\omega^2 + p_i^2} \right) - j \left(\sum_{i=1}^{\vartheta} \frac{K_i \omega}{\omega^2 + p_i^2} \right). \tag{13}$$

For real and complex conjugate poles, the quantities in the parenthesis of (13) are real. This leads to the linear system of equations shown in (14) at the bottom of the following page. The solution of (14) gives the partial fraction expansion coefficient matrices K_i's.

IV. Procedure for Time-Domain Measurements

A. Determining the Order of the Pole-Residue Model

Proper order selection is an essential criterion for automatic generation of a pole-residue representation of a network function. This order selection is a difficult task. The choice of a reasonable value for the approximation order is important in increasing simulation efficiency. In general, a low order may result in the loss of some useful features or even in inaccurate approximation, and on the other hand, an overly large order may increase oscillation from spurious modes appearing. Since the shape of the original waveform can be represented by two points between maxima, the initial guess for the order of the rational function is set to twice the number of maxima of the real or magnitude part of the frequency-domain data. First, however,

$$\begin{bmatrix} 1 & T_0^2 & \cdots & T_0^{2\varepsilon} & -T_0^2\mathrm{Re}(S(\omega_0)) & \cdots & -T_0^{2\vartheta}\mathrm{Re}(S(\omega_0)) \\ 1 & T_1^2 & \cdots & T_1^{2\varepsilon} & -T_1^2\mathrm{Re}(S(\omega_1)) & \cdots & -T_1^{2\vartheta}\mathrm{Re}(S(\omega_1)) \\ \vdots & \vdots & \ddots & \vdots & \vdots & \ddots & \vdots \\ 1 & T_{k-1}^2 & \cdots & T_{k-1}^{2\varepsilon} & -T_{k-1}^2\mathrm{Re}(S(\omega_{k-1})) & \cdots & -T_{k-1}^{2\vartheta}\mathrm{Re}(S(\omega_{k-1})) \end{bmatrix} \begin{bmatrix} \tilde{A}_0 \\ \tilde{A}_1 \\ \vdots \\ \tilde{A}_\varepsilon \\ \tilde{b}_1 \\ \vdots \\ \tilde{b}_\vartheta \end{bmatrix} = \begin{bmatrix} \mathrm{Re}(S(\omega_0)) \\ \mathrm{Re}(S(\omega_1)) \\ \mathrm{Re}(S(\omega_2)) \\ \vdots \\ \mathrm{Re}(S(\omega_{k-1})) \end{bmatrix} \tag{12}$$

a three-point moving average is used to smooth the data, and then twice the number of extrema is taken as an initial guess to the order of the rational function. After determining the initial guess to the order, the poles are determined using (9) or (12). The residues are then solved using (14), and the order is iteratively refined to meet the error criterion. For nonband-limited data, windowing is first used to reduce the energy leakage at $\omega_{\max}$. A detailed description on the effects of various windows when used with DFT can be found in [17].

B. Determining the Poles

Although (9) is a notoriously ill-conditioned system of equations, for many practical problems it can be solved accurately by simply normalizing the frequency so that the range of approximation maps to $[-1, 1]$ by using a change of variables

$$\tilde{\omega} = \frac{\omega - \frac{1}{2}(\omega_{\max} + \omega_{\min})}{\frac{1}{2}(\omega_{\max} - \omega_{\min})}. \tag{15}$$

The condition of the problem is improved by using Chebyshev polynomials, as in (12). The minimum number of points for the interpolation is $k = n$. Since the number of unknowns is often greater than n, (9) and (12) can be transformed into a square matrix using the method of average [13]. The method of average is used to obtain a consistent system of equations by adding consecutive equations in (9) and (12) into n groups. This averages the random error in the measurement noise, thus making the interpolation process less sensitive to noise.

The interpolation is made less sensitive to measurement error and noise by extracting common poles to all scattering parameters of an n-port. The pole-residue models of the scattering parameters share the same poles because the poles are physical attributes of the system and they are common to all scattering parameters. Therefore, the poles are extracted only once using data from all the scattering parameters. Once the poles of the S-matrix are determined, the residues are calculated for each scattering parameter.

C. Determining the Residues

After the polynomial roots are determined, if purely imaginary poles are present, they are rejected as spurious. The remaining poles with negative real parts are used with the original frequency-domain data to determined the residue values using (14). The renormalized frequencies can be used in (14) since the matrix is well conditioned. The residues K of an n-port scattering matrix consists of K_{ij}, where $i, j = 1, 2, \ldots, n$. For an n-port scattering matrix, solving (14) for each residue of the scattering matrix S_{ij} improves the efficiency and accuracy of the approximations.

If the measurement is also done at dc, i.e., $\omega_0 = 0$, it is important to remove $\mathrm{Im}(S(\omega_0))$ from the right-hand side and the corresponding row form the left-hand side of (14). The magnitude of the error between the original data and the pole-residue model values is calculated. If the error is below the threshold, the coefficients are stored or updated and the degree of the model is decreased and the approximation process is repeated. If the error is above the threshold and there are no coefficients stored, the degree is increased and the approximation process is repeated. If the error is acceptable or there are coefficients stored that give error below the threshold, the approximation is completed. The pole-residue pairs can then be used to generate the time-domain response of the network.

Although the method is applicable to arbitrarily spaced samples, the accuracy of the approximation can decrease when the ratio of the largest interval to the smallest interval is very large.

V. Experimental Results

A Beatty standard structure and a low-pass Butterworth filter are given to demonstrate the accuracy of the proposed method. The calculated time-domain impulse responses are compared with the data from measurement and conventional

$$\begin{bmatrix} 1 & \frac{-p_1}{\omega_0^2+p_1^2} & \cdots & \frac{-p_\vartheta}{\omega_0^2+p_\vartheta^2} \\ 1 & \frac{-p_1}{\omega_1^2+p_1^2} & \cdots & \frac{-p_\vartheta}{\omega_1^2+p_\vartheta^2} \\ \vdots & \vdots & \cdots & \vdots \\ 1 & \frac{-p_1}{\omega_{k-1}^2+p_1^2} & \cdots & \frac{-p_\vartheta}{\omega_{k-1}^2+p_\vartheta^2} \\ 0 & \frac{-\omega_0}{\omega_0^2+p_1^2} & \cdots & \frac{-\omega_0}{\omega_0^2+p_\vartheta^2} \\ 0 & \frac{-\omega_1}{\omega_1^2+p_1^2} & \cdots & \frac{-\omega_1}{\omega_1^2+p_\vartheta^2} \\ \vdots & \vdots & \ddots & \vdots \\ 0 & \frac{-\omega_{k-1}}{\omega_{k-1}^2+p_1^2} & \cdots & \frac{-\omega_{k-1}}{\omega_{k-1}^2+p_\vartheta^2} \end{bmatrix} \begin{bmatrix} K_0 \\ K_1 \\ K_2 \\ \vdots \\ K_\vartheta \end{bmatrix} = \begin{bmatrix} \mathrm{Re}(S(\omega_0)) \\ \mathrm{Re}(S(\omega_1)) \\ \vdots \\ \mathrm{Re}(S(\omega_{k-1})) \\ \mathrm{Im}(S(\omega_0)) \\ \mathrm{Im}(S(\omega_1)) \\ \vdots \\ \mathrm{Im}(S(\omega_{k-1})) \end{bmatrix} \tag{14}$$

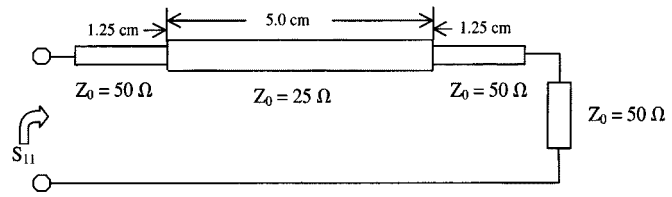

Fig. 3. One-port measurement of the Beatty standard structure terminated with a matched load.

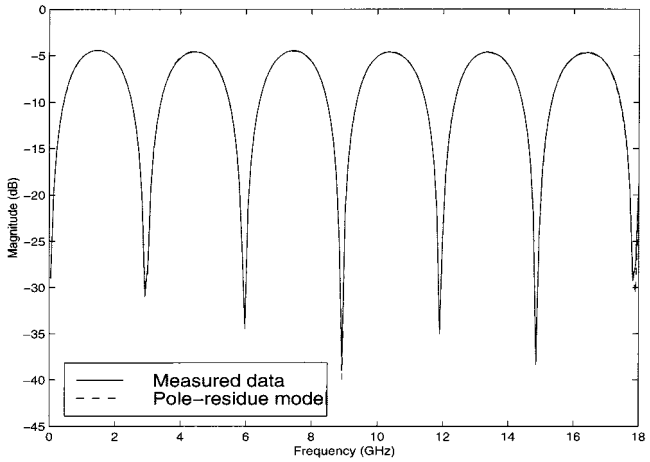

Fig. 4. Magnitude plots of S_{11} of the Beatty standard from 45 MHz to 18 GHz, the measured raw data, and the 24th-order pole-residue model.

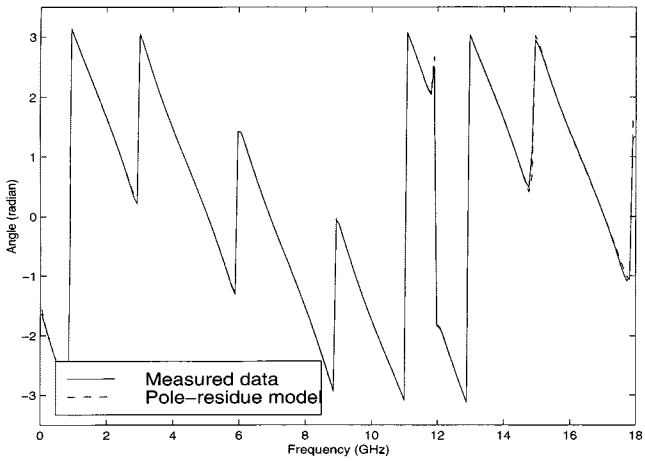

Fig. 5. Phase plots of S_{11} of the Beatty standard from 45 MHz to 18 GHz, the measured raw data, and the 24th-order pole-residue model.

methods. Note that the following examples have very complex frequency-domain responses that can be extremely difficult to model using standard global approximation methods without resorting to optimization techniques.

Example 1: First, the Beatty standard terminated with 50 Ω (similar to the one in [4]), which is shown in Fig. 3, is considered. The structure has two impedance step discontinuities that can give rise to reflections. The Agilent 8510B vector-network analyzer is used to measure the S_{11}-parameter from 45 MHz to 18 GHz using 201 points. The S_{11}-parameter data is approximated using 24th-order pole-residue model. The magnitude and phase responses of the data from measurement and pole-residue model are given in Figs. 4 and 5, respectively. By applying an

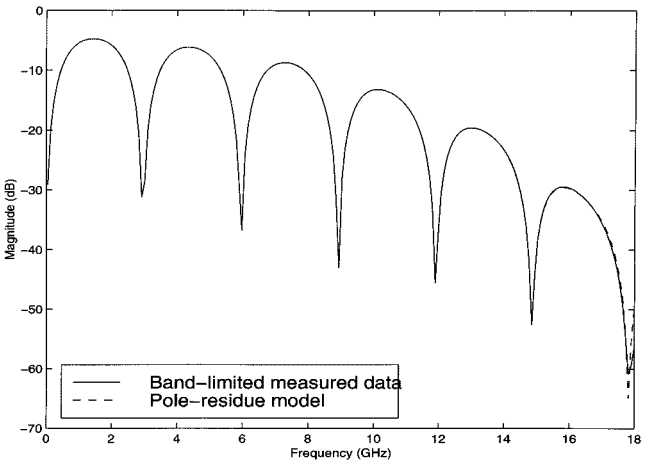

Fig. 6. Magnitude plots of S_{11} of the Beatty standard from 45 MHz to 18 GHz, the band-limited measured data, and the 20th-order pole-residue model.

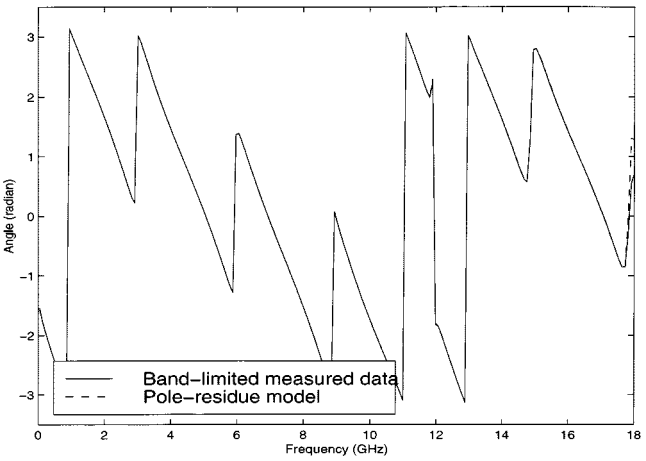

Fig. 7. Phase plots of S_{11} of the Beatty standard from 45 MHz to 18 GHz, the band-limited measured data, and the 20th-order pole-residue model.

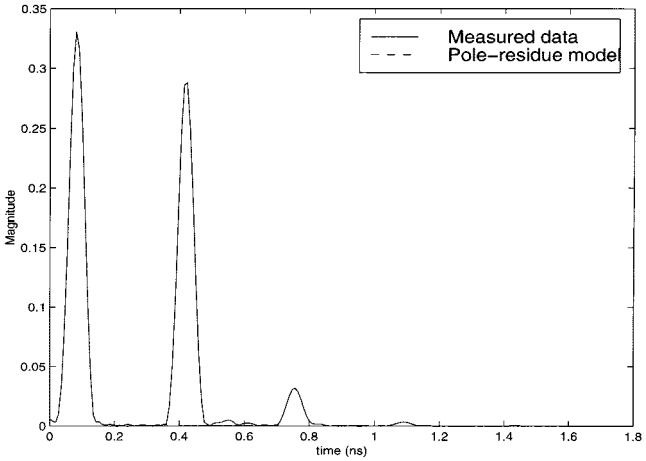

Fig. 8. Magnitude plots of the impulse responses of the Beatty standard using inverse FFT and the 20th-order pole-residue model of the band-limited measured data.

appropriate window, these pole-residue models can be used to calculate the time-domain response.

Alternatively, the impulse response can be obtained; first, the S_{11} data is band limited with windowing to reduce any energy leakage. A Kaiser window with window constant $\alpha = 6.0$ is

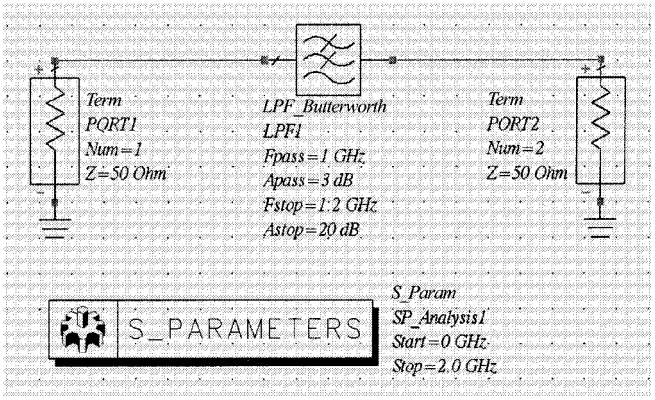

Fig. 9. Schematic of a two-port scattering parameter analysis of a Butterworth filter in the Agilent ADS.

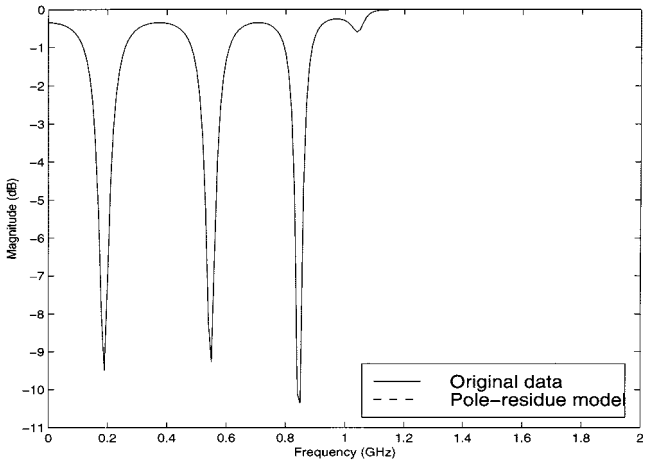

Fig. 10. Magnitude plots of S_{11} of the low-pass Butterworth filter from 0 Hz to 2 GHz, the original data, and the 12th-order pole-residue model.

used in order to make a direct comparison to Agilent 8510B time-domain option internal techniques. The band-limited S_{11} is then approximated by a 20th-order pole-residue model. The magnitude and phase responses of the band-limited data from the measurement and pole-residue model are given in Figs. 6 and 7, respectively. The pole-residue model of the band-limited S_{11} is then used to generate the impulse response of the Beatty structure using the analytical Laplace inversion . The comparison of the impulse responses between Agilent 8510B and the pole-residue model constructed using the Kaiser-windowed frequency-domain data are given in Fig. 8. The pole-residue model shows a perfect agreement to the impulse response from Agilent 8510B.

Example 2: The proposed method can also be applied to calculate the time-domain response of a two-port S-parameter simulation data of a 13th-order low-pass Butterworth filter. The filter has a cutoff and stopband frequencies of 1.0 and 1.2 GHz, respectively. The filter is characterized by 201 equally spaced frequency-domain data. The scattering parameters are computed using the S-parameter simulation controller available in the Agilent Advanced Design System (ADS) simulator [18]. The ADS schematic for the scattering parameter analysis of the Butterworth filter is shown in Fig. 9.

A 12th-order pole-residue models are constructed to represent the scattering parameters S_{11} and S_{21}. Since these pole-residue models share the same poles, they are extracted using

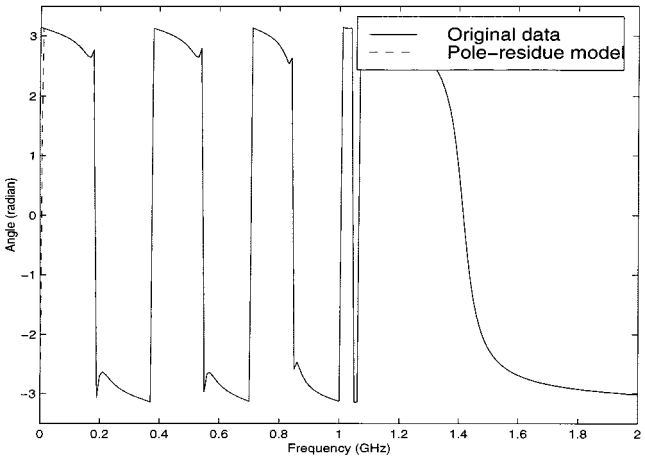

Fig. 11. Phase plots of S_{11} of the low-pass Butterworth filter from 0 Hz to 2 GHz, the original data, and the 12th-order pole-residue model.

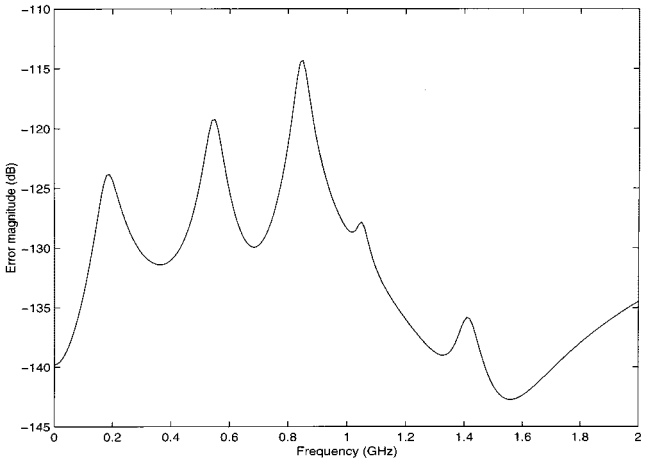

Fig. 12. Magnitude plots of the error of 12th-order pole-residue model of S_{11} of the low-pass Butterworth filter.

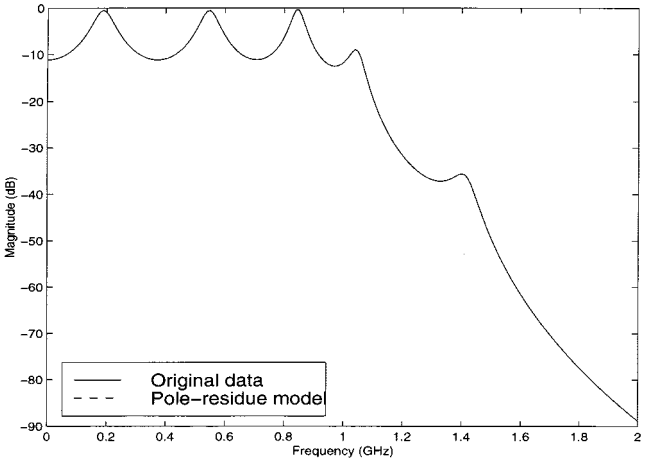

Fig. 13. Magnitude plots of S_{21} of the low-pass Butterworth filter from 0 Hz to 2 GHz, the original data, and the 12th-order pole-residue model.

(9) and the residues are calculated for each scattering parameters using (14). The magnitude and phase of the original and approximated S_{11}-parameter are shown in Figs. 10 and 11, respectively. The relative error in the approximation is lower than -110 dB, as shown in Fig. 12.

The magnitude and phase of the original and approximated S_{21}-parameter are shown in Figs. 13 and 14, respectively. The

TABLE I
POLE-RESIDUE PAIRS OF S_{21} FOR EXAMPLE 2. THERE IS NO POLE CORRESPONDING TO THE FINAL VALUE, $[k_{11}]_0$, IN THE FIRST ROW

No	Residues	Poles
0	$1.1306525768432705 \times 10^{-10} + j5.0528024220353709 \times 10^{-16}$	
1	$4.2720938713147634 \times 10^{3} \pm j9.5595312152511429 \times 10^{2}$	$-2.0695508562021252 \times 10^{9} \pm j1.6597007774625940 \times 10^{10}$
2	$-1.0648421121032103 \times 10^{6} \mp j3.6920227015404783 \times 10^{6}$	$-2.4142057223284885 \times 10^{8} \pm j8.8832672222893709 \times 10^{9}$
3	$8.2300639825588604 \times 10^{6} \pm j5.8152545492169683 \times 10^{7}$	$-1.6437929724653038 \times 10^{8} \pm j6.5810010541544868 \times 10^{9}$
4	$-9.3854672428885131 \times 10^{6} \mp j1.4373386927933698 \times 10^{8}$	$-1.4497009798937341 \times 10^{8} \pm j5.3146478698263442 \times 10^{9}$
5	$3.2536463476569777 \times 10^{6} \pm j1.9519748715434471 \times 10^{8}$	$-2.0385149840838013 \times 10^{8} \pm j3.4390505508621674 \times 10^{9}$
6	$-1.0376740239682891 \times 10^{6} \mp j2.1718814712946717 \times 10^{8}$	$-2.2680343184509462 \times 10^{8} \pm j1.1855694290586274 \times 10^{9}$

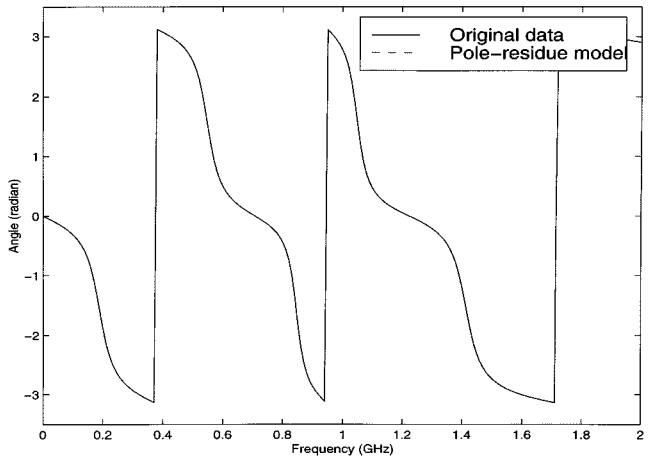

Fig. 14. Phase plots of S_{21} of the low-pass Butterworth filter from 0 Hz to 2 GHz, the original data, and the 12th-order pole-residue model.

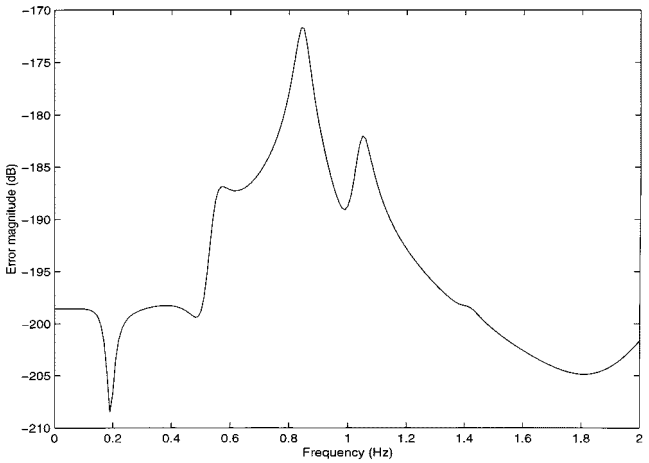

Fig. 15. Magnitude plots of the error of 12th-order pole-residue model of S_{21} of the low-pass Butterworth filter.

relative error in the approximation is lower than -170 dB, as shown Fig. 15.

The original S_{21} data is self-windowing, therefore, its pole-residue model is directly used to generate the impulse response of the filter. The comparison of the impulse responses between the conventional method and proposed pole-residue model are given in Fig. 16. The two time-domain impulse responses are indistinguishable. The pole-residue pairs for S_{21} of the Butterworth filter is given in Table I.

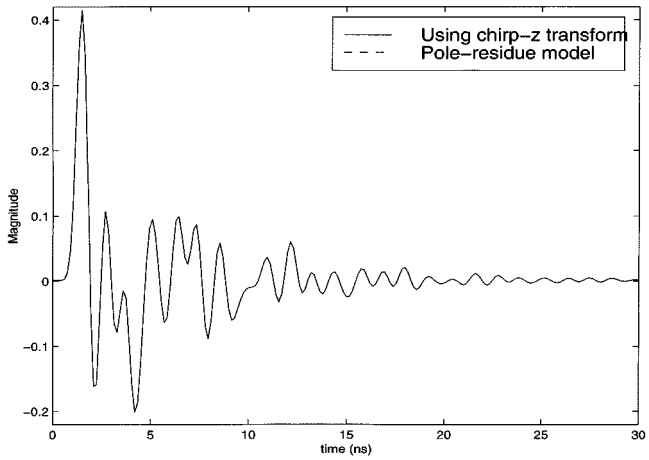

Fig. 16. Plots of the impulse responses of the low-pass Butterworth filter using inverse FFT and the 12th-order pole-residue model of the original data.

VI. CONCLUSIONS

An efficient and accurate technique for calculating a time-domain response from frequency-domain measurement data obtained from a network analyzer has been presented in this paper. The method generates an accurate pole-residue representation of the frequency-domain measurement and uses an analytical inversion formula of Laplace transform to construct the corresponding time-domain waveform. The frequency-domain data can be arbitrarily spaced and have a relatively small number of points. The method provides a fast way to view an alias-free time-domain waveform in any given time window. Thus, for many applications, the approach can be more efficient and more accurate than the conventional method that uses an IDFT to estimate the time-domain response from a large number of equally spaced harmonically related frequency points. The complexity of the method is the solutions of two linear systems of equations and the factorization of the roots of a real polynomial.

The method provides the ability for a network analyzer to extract pole-residue or pole-zero models and to simulate traditional TDR and TDT by taking advantage of the wide dynamic range and error correction associated with the frequency-domain measurement or data. We have used the technique successfully on data from network analyzer measurement and an RF/analog simulator. The examples show that the proposed method is very accurate in both the time and frequency domains. For many examples, the magnitude and phase waveforms of the data from measurement and pole-residue model were indistinguishable.

The generated pole-residue models, even for very complex frequency-domain data, were of a relatively low order. In addition, the pole-residue representation can be used to efficiently store measurement data with a large number of samples. The pole-residue models can also be used in a simulation or optimization program [18] to reduce the computational time by several order of magnitude while preserving accuracy.

ACKNOWLEDGMENT

The author would like to thank Dr. P. O'Halloran, Agilent Technologies, Santa Rosa, CA, and Prof. J. Schutt-Ainé, University of Illinois at Urbana-Champaign, for their valuable comments and suggestions, as well as Project Manager Dr. B. Troyanovsky, Agilent Technologies, Santa Rosa, CA, for supporting this paper.

REFERENCES

[1] M. E. Hines and H. E. Stinehelfer, Sr., "Time-domain oscillographic microwave network analysis using frequency-domain data," *IEEE Trans. Microwave Theory Tech.*, vol. MTT-22, pp. 276–282, Mar. 1974.

[2] *Agilent 8510 Network Analyzer Operating and Programming Manual*, Agilent Technol., Santa Rosa, CA, 1984.

[3] B. Ulriksson, "Conversion of frequency-domain data to the time domain," *Proc. IEEE*, vol. 74, pp. 74–77, Jan. 1986.

[4] Z. A. Marićević, T. K. Sarkar, Y. Hua, and A. R. Dijordević, "Time-domain measurements with the Hewlett-Packard network analyzer HP8510 using the matrix pencil method," *IEEE Trans. Microwave Theory Tech.*, vol. 39, pp. 538–547, Mar. 1991.

[5] H. Van hamme, "High-resolution frequency-domain reflectometry by estimation of modulated superimposed complex sinusoids," *IEEE Trans. Instrum. Meas.*, vol. 41, pp. 762–767, Dec. 1992.

[6] T. Karle and C. Reuter, "Time domain analysis of high frequency circuits through measurement-based characterization parametric techniques," in *Proc. Summer Comput. Simulat. Conf.*, Arlington, VA, July 13–17, 1997, pp. 410–413.

[7] Z. A. Samant and S. Shearman, "High-resolution frequency analysis with a small data record," *IEEE Spectr.*, vol. 36, pp. 82–86, Sept. 1999.

[8] J. Umoto and T. Hara, "A new digital analysis of surge performance in electric power networks utilizing the convolution integral," *J. Inst. Elect. Eng. Japn.*, vol. 91, no. 3, pp. 48–57, 1971.

[9] Z. A. Semlyen and A. Dabuleanu, "Fast and accurate switching transient calculations on transmission lines with ground return using recursive convolutions," *IEEE Trans. Power App. Syst.*, vol. PAS-94, pp. 561–571, Mar./Apr. 1975.

[10] A. V. Oppenheim and R. W. Schafer, *Discrete-Time Signal Processing*. Englewood Cliffs, NJ: Prentice-Hall, 1989.

[11] J. D. Jackson, *Classical Electrodynamics*, 2nd ed. New York: Wiley, 1975.

[12] A. Papoulis, *The Fourier Integral and Its Applications*. New York: MGraw-Hill, 1962.

[13] D. B. Kuznetsov and J. E. Schutt-ainé, "Optimal transient simulation of transmission lines," *IEEE Trans. Circuits Syst. I*, vol. 43, pp. 111–121, Feb. 1996.

[14] W. T. Beyene and J. E. Schutt-ainé, "Efficient transient simulation of high-speed interconnect characterized by sampled data," *IEEE Trans. Comp., Hybrids, Manufact. Technol.*, vol. 21, pp. 105–114, Nov. 1998.

[15] J. Adcock, "Curve fitter for pole-zero analysis," *Hewlett-Packard J.*, vol. 37, no. 1, pp. 33–36, Jan. 1987.

[16] W. H. Press, S. A. Teukolsky, W. T. Vetterling, and B. P. Flannery, *Numerical Recipes in C: The Art of Scientific Computing*, 2nd ed. Oxford, U.K.: Cambridge Univ. Press, 1992.

[17] F. J. Harris, "On the use of window for harmonic analysis with the discrete Fourier transform," *Proc. IEEE*, vol. 66, pp. 51–83, Jan. 1970.

[18] *Advanced Design System User's Guide*, Agilent Technol., Santa Rosa, CA, Nov. 1999.

Wendemagegnehu T. Beyene (S'87–M'88) was born in Addis Ababa, Ethiopia. He received the B.S. and M.S. degrees in electrical engineering from Columbia University, New York, NY, in 1988 and 1991 respectively, and the Ph.D. degree in electrical and computer engineering from the University of Illinois at Urbana-Champaign, in 1997.

From 1988 to 1994, he was with the Microelectronics Division, IBM, East Fishkill, NY, where he was involved with the design, electrical analysis, and characterization of advanced electronic packages. In 1997, he joined the EEsof Division, Hewlett-Packard Company, where he was involved with analog/RF circuits simulation tools for Agilent Technologies, Westlake Village, CA. He is currently with Rambus Inc., Los Altos, CA. His professional interests include analog/RF circuit and system simulation techniques, field simulation of devices and electromagnetic systems, very large scale integration (VLSI) interconnects and RF packaging analyses, as well as their measurements.

Dr. Beyene is a member of Eta Kappa Nu, Tau Beta Pi, and the Society for Industrial and Applied Mathematics (SIAM).